frontiers in Pharmacology

ORIGINAL RESEARCH
published: 18 January 2022
doi: 10.3389/fphar.2021.794620

Investigation of the Effects of the Short QT Syndrome D172N Kir2.1 Mutation on Ventricular Action Potential Profile Using Dynamic Clamp

Chunyun Du[1], *Randall L. Rasmusson*[2,3], *Glenna C. Bett*[2,3,4], *Brandon Franks*[3], *Henggui Zhang*[5] *and Jules C. Hancox*[1,5]*

[1]School of Physiology, Pharmacology and Neuroscience, University of Bristol, Bristol, United Kingdom, [2]Department of Physiology and Biophysics, Jacobs School of Medicine and Biomedical Sciences, University of New York, University at Buffalo, Buffalo, NY, United States, [3]Cytocybernetics Inc, North Tonawanda, NY, United States, [4]Department of Obstetrics and Gynecology, Center for Cellular and Systems Electrophysiology, State University of New York, University at Buffalo, Buffalo, NY, United States, [5]Biological Physics Group, Department of Physics and Astronomy, The University of Manchester, Manchester, United Kingdom

OPEN ACCESS

Edited by:
Saïd Bendahhou,
University of Nice Sophia Antipolis, France

Reviewed by:
Flavien Charpentier,
INSERM U1087 L'unité de Recherche de L'institut du Thorax, France
Ronald Wilders,
University of Amsterdam, Netherlands

***Correspondence:**
Jules C. Hancox
jules.hancox@bristol.ac.uk

Specialty section:
This article was submitted to Pharmacology of Ion Channels and Channelopathies, a section of the journal Frontiers in Pharmacology

Received: 13 October 2021
Accepted: 14 December 2021
Published: 18 January 2022

Citation:
Du C, Rasmusson RL, Bett GC, Franks B, Zhang H and Hancox JC (2022) Investigation of the Effects of the Short QT Syndrome D172N Kir2.1 Mutation on Ventricular Action Potential Profile Using Dynamic Clamp. Front. Pharmacol. 12:794620. doi: 10.3389/fphar.2021.794620

The congenital short QT syndrome (SQTS) is a cardiac condition that leads to abbreviated ventricular repolarization and an increased susceptibility to arrhythmia and sudden death. The SQT3 form of the syndrome is due to mutations to the *KCNJ2* gene that encodes Kir2.1, a critical component of channels underlying cardiac inwardly rectifying K^+ current, I_{K1}. The first reported SQT3 *KCNJ2* mutation gives rise to the D172N Kir2.1 mutation, the consequences of which have been studied on recombinant channels *in vitro* and in ventricular cell and tissue simulations. The aim of this study was to establish the effects of the D172N mutation on ventricular repolarization through real-time replacement of I_{K1} using the dynamic clamp technique. Whole-cell patch-clamp recordings were made from adult guinea-pig left ventricular myocytes at physiological temperature. Action potentials (APs) were elicited at 1 Hz. Intrinsic I_{K1} was inhibited with a low concentration (50 μM) of Ba^{2+} ions, which led to AP prolongation and triangulation, accompanied by a ~6 mV depolarization of resting membrane potential. Application of synthetic I_{K1} through dynamic clamp restored AP duration, shape and resting potential. Replacement of wild-type (WT) I_{K1} with heterozygotic (WT-D172N) or homozygotic (D172N) mutant formulations under dynamic clamp significantly abbreviated AP duration (APD_{90}) and accelerated maximal AP repolarization velocity, with no significant hyperpolarization of resting potential. Across stimulation frequencies from 0.5 to 3 Hz, the relationship between APD_{90} and cycle length was downward shifted, reflecting AP abbreviation at all stimulation frequencies tested. In further AP measurements at 1 Hz from hiPSC cardiomyocytes, the D172N mutation produced similar effects on APD and repolarization velocity; however, resting potential was moderately hyperpolarized by application of mutant I_{K1} to these cells. Overall, the results of this study support the major changes in ventricular cell AP repolarization with the D172N predicted from prior AP modelling and highlight the potential utility of using adult ventricular cardiomyocytes for dynamic clamp exploration of functional consequences of Kir2.1 mutations.

Keywords: arrhythmia, dynamic clamp, KCNJ2, Kir2.1, short QT syndrome, ventricular myocyte

INTRODUCTION

Cardiac action potential (AP) repolarization depends on the dynamic interplay between multiple ionic currents, including those carried by a number of key potassium channels (Varro et al., 2020). Thus, early repolarization of ventricular APs is influenced by the rapidly activating and inactivating transient outward potassium current, I_{TO} (Tamargo et al., 2004; Varro et al., 2020), whilst the rapid and slow delayed rectifier potassium currents (I_{Kr} and I_{Ks}) contribute to repolarization over AP plateau voltages (Mitcheson and Sanguinetti, 1999; Tamargo et al., 2004; Varro et al., 2020). The terminal phase of ventricular AP repolarization is substantially driven by the inwardly rectifying K^+ current, I_{K1} (Tamargo et al., 2004; Varro et al., 2020). Early application of the AP voltage clamp technique to rabbit ventricular myocytes showed that I_{K1} is suppressed at AP plateau voltages, but increases steeply during the late phase of the AP, peaking negative to ~ −60 mV, before then declining as the AP voltage approaches the K^+ equilibrium potential (Shimoni et al., 1992). From work on guinea-pig ventricular myocytes Ishihara and Ehara suggested that the increase in outward I_{K1} during repolarization involves relief of block of the underlying channels by intracellular Mg^{2+} ions (Ishihara and Ehara, 1998). The relative timing of ventricular I_{Kr} and I_{K1} ensures that as the former current declines, the latter increases, assuming the dominant role in final repolarization (Mitcheson and Hancox, 1999; Banyasz et al., 2011; Horvath et al., 2021). Functional I_{K1} channels are comprised of tetramers of Kir2.x α subunits (Dhamoon and Jalife, 2005; Hibino et al., 2010; Varro et al., 2020). *KCNJ2* is responsible for Kir2.1 which is strongly expressed in human atria and ventricles (Wang et al., 1998; Gaborit et al., 2007). The importance of Kir2.1 in contributing to native I_{K1} is demonstrated by the fact that loss-of-function *KCNJ2* mutations have been implicated in Andersen-Tawil syndrome, which causes one form of long QT syndrome (long QT type 7) as well as extra-cardiac abnormalities (Tristani-Firouzi and Etheridge, 2010; Perez-Riera et al., 2021). Conversely, over-expression of Kir2.1 in the mouse heart produces a substrate favourable to high-frequency rotor development and rotor stabilization (Noujaim et al., 2007). Moreover, gain-of-function *KCNJ2* mutations have been implicated in human familial atrial fibrillation (Xia et al., 2005) and the SQT3 variant of the short QT syndrome (SQTS; Priori et al., 2005; Hattori et al., 2012; Deo et al., 2013; Ambrosini et al., 2014).

The congenital SQTS is characterized by abbreviated QT intervals, (often) tall upright T waves and increased susceptibility to ventricular arrhythmias (Maury et al., 2008; Hancox et al., 2018). The SQT3 *KCNJ2* missense mutations thus far identified impair Kir2.1 current rectification, with the consequence that outward I_{K1} is augmented and thereby makes a greater contribution to AP repolarization (Hancox et al., 2018; Hancox et al., 2019). The first reported SQT3 Kir2.1 mutation (D172N) was identified in an asymptomatic 5-year old girl with an abnormal electrocardiogram, whose father had a history of presyncopal events and palpitations (Priori et al., 2005). Both father and daughter had markedly abbreviated QT_c intervals (320 ms) and asymmetric T waves (Priori et al., 2005). The D172 residue is located in the Kir2.1 pore and is involved in polyamine and Mg^{2+} block of the channel that gives rise to voltage dependent rectification (Abrams et al., 1996; Priori et al., 2005). The D172N mutation impairs this process, resulting in a preferential augmentation of outward current (Priori et al., 2005; El Harchi et al., 2009). Simulations incorporating the consequent change to I_{K1} have shown action potential and QT interval shortening and increased tissue vulnerability to atrial and ventricular arrhythmias (Priori et al., 2005; Adeniran et al., 2012; Whittaker et al., 2017). The M301K and E299V Kir2.1 SQT3 mutations impair Kir2.1 current rectification to greater extents than does D172N (Hattori et al., 2012; Deo et al., 2013).

There are at present no genotypically accurate experimental models of SQT3 and therefore information on the functional consequence of SQT3 mutations has almost exclusively derived from electrophysiological studies of recombinant channels and computational modelling (Priori et al., 2005; El Harchi et al., 2009; Adeniran et al., 2012; Hattori et al., 2012; Deo et al., 2013; Ambrosini et al., 2014; Whittaker et al., 2017). Patient-specific human induced pluripotent stem cell derived cardiomyocytes (hiPSC-CMs) have recently been used to study *KCNH2* mutation linked SQT1 variants of the SQTS (El-Battrawy et al., 2018; Guo et al., 2018). However, iPSC-CMs tend to exhibit an immature spontaneously active phenotype in which I_{K1} is sparse or absent (Doss et al., 2012; Hoekstra et al., 2012) and so are not as readily used to study mutations that affect I_{K1}. Adenoviral transduction with Kir2.1 provides one potential solution to this problem (Lieu et al., 2013; Jones et al., 2014), although precise titration of wild-type and mutant channel subunits to compare homozygous and heterozygous expression conditions represents a technical challenge. An alternative approach is to supply a "virtual" I_{K1} electronically using the "dynamic clamp" method (Bett et al., 2013). The real-time application of virtual I_{K1} has been shown to improve hiPSC-CM AP configuration in both manual and automated patch clamp approaches (Bett et al., 2013; Meijer van Putten et al., 2015; Goversen et al., 2017; Verkerk et al., 2017; Becker et al., 2020). Moreover, Meijer van Putten and others adopted this approach to show hiPSC-CM AP changes with simulated loss of I_{K1} (mimicking Andersen-Tawil syndrome) and of increased I_{K1} due to the effects of the E299V SQT3 mutation (which produced marked AP abbreviation; Meijer van Putten et al., 2015). Although hiPSC-CMs have the advantage of their human origin, they nonetheless retain the drawback of lack of maturity. Consequently, a complementary approach is the use of adult ventricular myocytes from an appropriate model species. Accordingly, the present study was undertaken to investigate the effects on adult guinea-pig ventricular myocyte AP configuration of real-time replacement of a wild-type I_{K1} with SQT3 (D172N) I_{K1}, using WT and mutant formulations for I_{K1} previously derived from experimental data and used for *in silico* cell and tissue models (El Harchi et al., 2009; Adeniran et al., 2012; Whittaker et al., 2017). Our findings

constitute a direct demonstration of causality between the D172N Kir2.1 mutation and abbreviated ventricular AP repolarization.

METHODS

Guinea-Pig Ventricular Myocyte Isolation

Adult male guinea-pigs (300–600 g) were killed in accordance with UK Home Office legislation. Left ventricular myocytes were then isolated by enzymatic and mechanical dispersion as described previously (Zhang et al., 2001; Ridley et al., 2003). Briefly, guinea-pigs were anaesthetized with pentobarbital sodium (140 mg/kg, I.P.) together with heparin (4,000 U/kg). The heart was removed quickly and was then cannulated and perfused with a Langendorff perfusion system at 37°C. The basic perfusion solution contained: 130 NaCl, 5.4 KCl, 5 HEPES, 10 Glucose, 0.4 NaH_2PO_4, 3 $MgCl_2$, 20 taurine and 10 creatine (pH 7.61 with NaOH). First, basic solution containing 750 μM of $CaCl_2$ was perfused for 2 min, then Ca^{2+}-free basic perfusion solution was supplied for 5 min, followed by low Ca^{2+} (150 μM) containing basic solution that also contained collagenase (Worthington, Type I, 0.3 mg/ml per100 g body weight) and protease (Merck, Type XIV 0.01 mg/ml per100 g body weight) for 4–7 min. Cells were then released from left ventricle by mechanical dispersion. Isolated myocytes were stored in low calcium solution (150 μM) at room temperature. Aliquots of the cell suspension were transferred into a chamber mounted on an inverted microscope and left to settle for several minutes, before being exposed to normal Tyrode solution. Only cells with a clear rod-shape and striated appearance were chosen for recording. The mean cell capacitance of guinea-pig ventricular myocytes used in this study was 98.3 ± 12.5 pF (12 myocytes from 8 hearts).

Culture of Cor.4U Human Induced Pluripotent Stem Cell Derived Cardiomyocytes

Cor.4U hiPSC-CMs were obtained from Axiogenesis (Nattermannallee, Köln, Germany). The cells were cultured according to the manufacturer's instructions for manual patch clamp experiments (MPC Protocol V1.1). Briefly, cells were thawed and suspended in culture medium (Axiogenesis) and seeded (20 μl at concentration of $5*10^4$ cells/ml) on gelatin (0.1%) coated glass shards in 12-well plates. After incubation at 37°C in 5% CO_2 for 3 h, the culture medium was added to the plates. The cells were kept in a 5% CO_2 incubator at 37°C with culture medium changed twice a week. Whole-cell patch clamp was conducted in weeks 2–3 of cell culture. The mean cell capacitance of hiPSC-CMs in this study was 56.8 ± 4.8 pF (n = 14 cells).

Electrophysiological Recording

Aliquots of adult guinea-pig left ventricular myocytes or glass shards with hiPSC-CMs were placed on the glass bottom of the chamber mounted on the microscope and the cells were continuously superfused at 37 ± 1°C with a standard Tyrode's solution containing (in mM): 140 NaCl, 4 KCl, 2 $CaCl_2$, 1 $MgCl_2$, 10 Glucose, 5 HEPES (titrated to pH 7.4 with NaOH; osmolarity 292 mOsm/L). For guinea-pig myocyte experiments, glass-pipettes (Corning 7,052 glass, AM Systems Inc.) were pulled with a horizontal micropipe puller (Sutter, P-97I) to give a resistance of 1–2 MΩ. For stem cell experiments, glass-pipettes were pulled with a vertical puller (Narishige, PP 830) and polished (Narishige, MF83) to give a final resistance of 2–3 MΩ. The pipette dialysis solution contained (in mM): 110 KCl, 10 NaCl, 5 MgATP, 0.4 $MgCl_2$, 10 HEPES, 5 Glucose. Pipette pH (and thereby bulk intracellular pH) was buffered to pH 7.2 with 10 mM HEPES (titrated with KOH, increasing pipette $[K^+]$ to 120 mM; osmolarity 248 mOsm/L). The theoretical potassium equilibrium potential (E_K) for these external and pipette solutions was −90.85 mV at 37°C. Series resistance values (typically 2–5 MΩ) were compensated by >70%. Transmembrane currents and action potentials were recorded in the whole-cell mode using an Axopatch 1D amplifier (Molecular Devices) and a CV-4 1/100 head stage. Data were recorded via a Digidata 1200B interface and stored on the hard-disk of a Viglen computer. Data digitization rates were 10 kHz during all protocols and an appropriate bandwidth of 2 kHz was set on the amplifier. Data acquisition (Clampex 8.2) and analysis (Clampfit 10.7) were performed using pCLAMP (Molecular Devices), Excel 365, Origin (2018 b) and GraphPad Prism (8) Software.

Dynamic Clamp

Dynamic clamp was carried out using a commercially available Cybercyte dynamic clamp system (Cybercyte V10) (Bett et al., 2013). The simulation system of the Cybercyte dynamic clamp consisted of a 16 channel, 16 bit, 100 kS/s MCC PCIe-DAS1602/16 board installed and configured in a Dell 5,810 Precision workstation. The average measured loop time for the system was 46 μs. The extracellular K concentration was set to 4 mM.

The model formulations for I_{K1} were based on the formulations of Adeniran et al. (2012) and are as follows:

$$I_{K1} = G_{K1}\sqrt{\frac{K_o}{5.4}}X_{K1\infty}(V - E_K)$$

$$\text{Where } X_{K1\infty} = \frac{\alpha_{K1}}{\alpha_{K1}+\beta_{K1}}$$

WT

$$\alpha_{K1} = \frac{0.07}{1 + e^{0.017(V-E_K-200.2)}}$$

$$\beta_{K1} = \frac{3e^{0.0003(V-E_K+100.2)} + e^{0.08(V-E_K-8.7)}}{1 + e^{-0.024(V-E_K)}}$$

$$G_{K1} = 4.8\,nS/pF$$

WT-D172N

$$\alpha_{K1} = \frac{0.1}{1 + e^{0.023(V-E_K-199.9)}}$$

$$\beta_{K1} = \frac{3e^{0.0002(V-E_K+100.4)} + e^{0.07(V-E_K-9.8)}}{1 + e^{-0.021(V-E_K)}}$$

$$G_{K1} = 8.26\,nS/pF$$

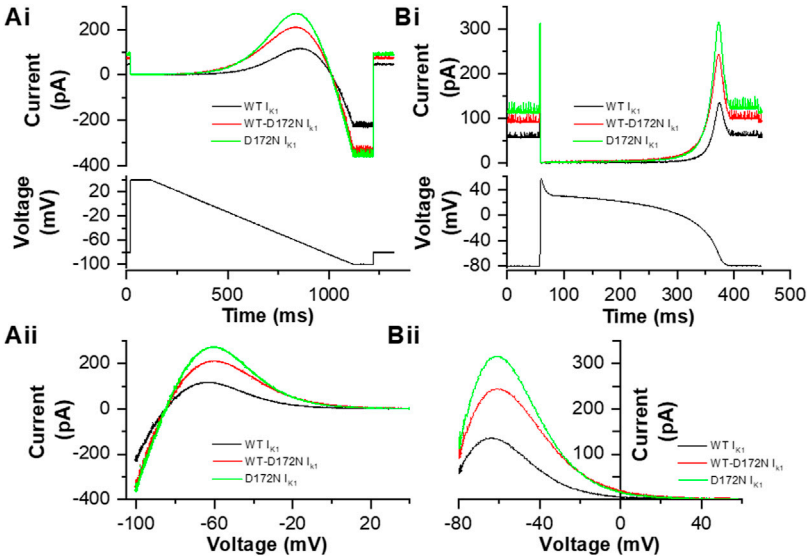

FIGURE 1 | I_{K1} formulations employed in this study. **Ai** Example current traces of WT I_{K1} (black), WT-D172N I_{K1} (red) and D172N I_{K1} (green) current derived from a conventional descending voltage ramp protocol shown in the lower panel, recorded from a model cell. **Aii**. I–V relations for WT, WT-D172N and D172N conditions. Peak outward I_{K1} during the descending voltage ramp occurred at −63.5, −60.5, and −60 mV respectively. **Bi.** Example current traces of WT I_{K1} (black), WT-D172N I_{K1} (red) and D172N I_{K1} (green) current derived from an action potential (AP) protocol shown in the lower panel, recorded from a model cell. **Bii.** Instantaneous I–V relations for WT, WT-D172N and D172N conditions during the AP repolarization phase (repolarization occurs from right to left on this plot). Peak outward current during AP repolarization occurred at −64, −60.5, and −60 mV respectively.

(1.72 fold the WT value).

D172N

$$\alpha_{K1} = \frac{0.1}{1 + e^{0.05\,(V - E_K - 199.9)}}$$

$$\beta_{K1} = \frac{3e^{0.0002\,(V - E_K + 100.1)} + e^{0.08\,(V - E_K - 10.3)}}{1 + e^{-0.006\,(V - E_K)}}$$

$$G_{K1} = 10.75\,nS/pF$$

(2.24 fold the WT value).

G_{K1} is the maximal conductance of I_{K1}; the values given above are exemplar starting values. In practice, the WT amplitude was scaled to produce an APD_{90} in Ba^{2+}-conditions that matched that in control Tyrode's solutions and the values for WT-D172N and D172N were then scaled accordingly (see next section). $X_{K1\infty}$ is the time-independent inward rectification factor that is a function of voltage; $\sqrt{\frac{K_o}{5.4}}$ is the K_o dependence of the current.

Testing the Dynamic Clamp Output

Prior to application of the dynamic clamp I_{K1} formulations to ventricular myocytes, an experiment was conducted in which the I_{K1} formulations to be used were applied in voltage clamp mode to a model cell (comprised of a 10 MΩ resistor and 500 MΩ resistor in series with one another, in parallel with a 33 pF capacitor in cell mode). **Figure 1Ai** shows WT, D172N and WT-D172N currents elicited by a descending voltage ramp (+40 to −100 mV over 1s). The Cytocybernetics system allows 1) current amplitude to be scaled as necessary during an experiment in order to provide an output of appropriate size; 2) the ratio of the different formulations to be fixed, so that these match experimentally derived values. Here, peak outward I_{K1} for D172N-WT was set to be 1.72 the WT current, whilst that for D172N was set to be 2.24 that for the WT current (estimated from **Figure 1A** of (Adeniran et al., 2012)). The corresponding current-voltage (I-V) relations are shown in **Figure 1Aii**, with I_{K1} reversing at −85 mV. This reversal potential for the I_{K1} formulation used in dynamic clamp was considered appropriate as it is close to that of−83.1 ± 0.6 mV reported for guinea-pig ventricular I_{K1} from perforated patch recordings by Ishihara et al. (2002) and is also near the reversal potential for Ba^{2+} sensitive I_{K1} in **Figure 2** of this study. As seen experimentally (Priori et al., 2005; El Harchi et al., 2009), outward current was larger and peaked at a more positive voltage for the D172N than the WT condition (by +3.5 mV compared to WT), with the D172N-WT condition intermediate in amplitude between the two (peak shifted by +3 mV compared to WT). Once these ratios had been set, an action potential (AP) clamp waveform was applied to the Cybercyte I_{K1} models of each condition using a simulated human ventricular AP waveform from the ten Tusscher et al. model (Ten Tusscher et al., 2004; McPate et al., 2009). The current outputs from the models during the AP command are shown in **Figure 1Bi**. As the holding potential (−80 mV) lay positive to E_{rev} there was outward holding current prior to the AP upstroke phase. A brief transient current was apparent during the AP upstroke and then little or no current flowed through part of the AP plateau, with a marked increase during late repolarization. **Figure 1Bii** shows the instantaneous I-V relation for I_{K1} during AP repolarization, with marked increases in current late in repolarization and current peaking

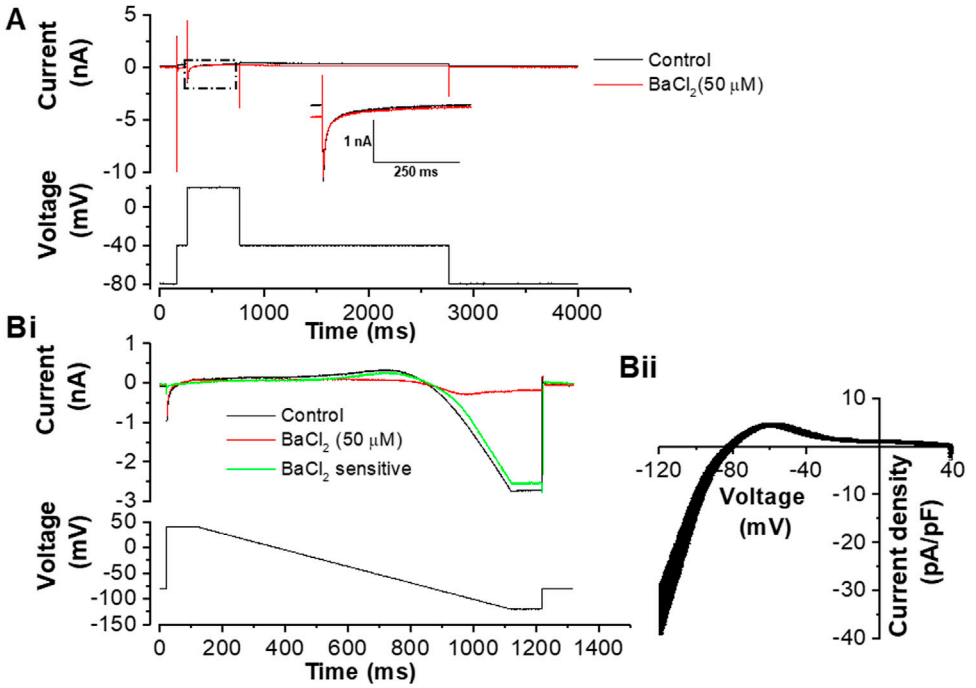

FIGURE 2 | Effects of 50 μM $BaCl_2$ on voltage clamped guinea-pig ventricular myocytes. **(A)**. Exemplar current traces (upper) elicited by the protocol shown in the lower panel. From a holding potential of −80 mV a step to −40 mV was applied to activate and inactivate fast sodium current (I_{Na}); this was followed by a step to +20 mV which elicited L-type Ca current ($I_{Ca,L}$). The black trace is in control and the red trace is in the presence of 50 μM $BaCl_2$. The inset shows expanded records of the portion of the traces marked by the dashed box, in order to aid visualization of $I_{Ca,L}$. **Bi**. Example current traces elicited by the protocol shown in the lower panel. The black trace is in control, red trace is with 50 μM of $BaCl_2$ and green trace is the $BaCl_2$ sensitive current. **Bii**. Mean ± SEM I-V plot of Ba^{2+}-sensitive current from 11 cells from 8 hearts (mean cell capacitance of 97.6 ± 13.7 pF). The measured reversal potential of this current was −81.6 ± 0.8 mV.

at a more positive voltage for D172N than WT current, with D172N-WT being intermediate (similar to the ramp current in **Figure 1Aii** and *cf* El Harchi et al., 2009). These observations confirmed that the current formulations could be applied in real-time and were as expected for the WT and mutant conditions to be studied subsequently under dynamic clamp.

Data are presented as mean ± SEM. Statistical tests used to evaluate statistical significance are given in the relevant Results text and were conducted using Microsoft Excel (Office 365), GraphPad PRISM 8.4.3 or GraphPad Instat 3.10. $p < 0.05$ was considered statistically significant.

RESULTS

Effects of Barium Block of I_{K1} on Ventricular AP Profile

In order to be able to replace endogenous I_{K1} with virtual I_{K1} via dynamic clamp, it was necessary to utilize an inhibitor of I_{K1}. In early experiments we attempted to use the pentamidine analogue PA-6 (1 μM; (Takanari et al., 2013)), but in our hands I_{K1} inhibition was slow to develop (*cf* Sanson et al., 2019) making it unsuitable for the purposes of this study. Instead, a low concentration of barium (Ba^{2+}) ions was used to inhibit I_{K1}. Native I_{K1} has been reported to be inhibited by Ba^{2+} with an IC_{50} of 4.7 μM (Schram et al., 2003) and the concentration used here (50 μM) was sufficient to block I_{K1} substantially without altering the amplitude or time-course of L-type calcium current ($I_{Ca,L}$) (**Figure 2**). **Figure 2A** shows representative $I_{Ca,L}$ records on step depolarization from −40 to +20 mV, with a K^+-based pipette dialysate: current during the step to +20 mV was unaltered, whereas the time-independent current at −40 mV was diminished, as expected for outward I_{K1} blockade. **Figure 2Bi** shows current during a descending ramp protocol in the absence and presence of Ba^{2+} ions, whilst **Figure 2Bii** shows the current-voltage (I-V) relation for Ba^{2+}-sensitive I_{K1} elicited by the ramp protocol. The Ba^{2+} sensitive I_{K1} density observed with this protocol at −120 mV was similar to that reported previously for guinea-pig ventricular I_{K1} elicited by a voltage step protocol (James et al., 2004).

Figure 3 shows the effect of Ba^{2+} ion application on the guinea-pig ventricular AP configuration and resting potential. For these experiments brief (2–10) ms suprathreshold depolarizing currents were applied to elicit APs (determined for each cell by progressive increase in current amplitude and or duration, up to a maximum of 10 ms in control conditions, then set to 100–200 pA above the threshold). **Figure 3A** shows representative APs elicited at 1 Hz (using a 3 ms injection of 1700 pA depolarizing current) in the absence and presence of Ba^{2+}. Control and $+Ba^{2+}$ APs were closely superimposed early during repolarization, but they diverged later in the AP plateau phase and terminal repolarization. The Poincaré plot in **Figure 3B** shows measurements of beat-to-beat variability (BVR) in APD_{90} in control solution and in the presence of I_{K1} inhibition by

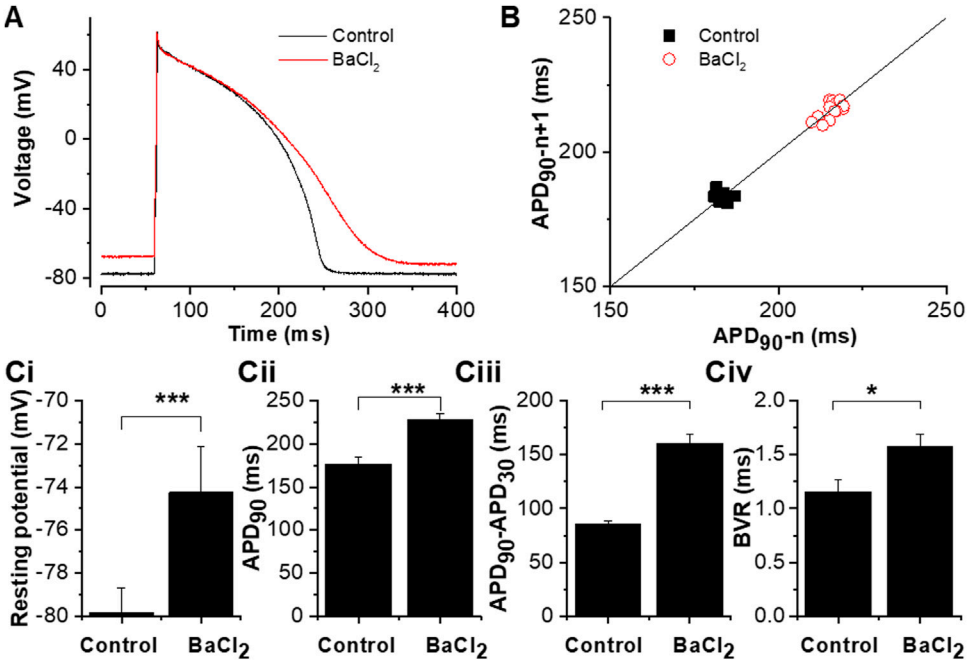

FIGURE 3 | Effects of 50 μM $BaCl_2$ on the guinea-pig ventricular action potential. **(A)**. The effect of 50 μM $BaCl_2$ on action potentials elicited from guinea-pig ventricular myocyte by brief (3 ms) suprathreshold (1700 pA) current pulses applied at 1 Hz (black trace in control and red trace in 50 μM $BaCl_2$). **(B)**. Poincaré plots of APD_{90} from 15 continuously action potentials showing the effect of $BaCl_2$ on beat-to-beat variability. Solid line shows line of identity (x = *y*). **Ci.** Effects of 50 μM $BaCl_2$ on the measured resting potential. **Cii.** Effects of 50 μM $BaCl_2$ on APD_{90} (for each cell, average APD_{90} values from 5 APs in each of control and Ba^{2+} conditions were obtained and then pooled). **Ciii**. Effects of 50 μM $BaCl_2$ on action potential triangulation (measured as the difference between APD_{90} and APD_{30}). **Civ.** Effects of 50 μM $BaCl_2$ on beat-to-beat variability [beat-to-beat variability was quantified as APD_{90} variability: $\sum(|APD_{90(n+1)} - APD_{90n}|)/(n*\sqrt{2})$, where APD_{90n} and $APD_{90(n+1)}$ indicated the APD_{90} durations of the *n*th and (n+1)th APs respectively. n denoted the number of consecutive bests analysed (15 here)]. "*" denotes statistical significance of $p < 0.05$; "***" denotes statistical significance of $p < 0.001$ (paired *t*-test, n = 12 cells from 8 hearts).

Ba^{2+}: variability appeared to be greater in the latter condition. **Figure 3C** shows mean data from 12 similar experiments. Resting potential (**Figure 3Ci**) was significantly depolarized in the presence of Ba^{2+} by ~ 6 mV (5.6 ± 1.1 mV; n = 12). APD_{90} was significantly increased (**Figure 3Cii**) and the difference between APD_{90} and APD_{30} (a measure of AP triangulation (Hondeghem et al., 2001)) was also significantly augmented by Ba^{2+} application. Evaluation of the APD_{30}/APD_{90} ratio from the same experiments was also consistent with augmented AP triangulation by Ba^{2+} ions (Control ratio of 0.51 ± 0.02 and of 0.31 ± 0.03 with Ba^{2+} application; $p < 0.0001$, paired *t*-test). BVR in APD was quantified as shown in **Figure 3Civ** (Valentin et al., 2004; Hancock et al., 2015) and was found to be significantly greater in the presence of Ba^{2+}. To summarise: I_{K1} inhibition with Ba^{2+} ions depolarized resting potential, increased APD_{90} and AP triangulation and augmented BVR.

Effects of the D172N Mutation Studied With Dynamic Clamp of Guinea-Pig Ventricular Myocytes

For experiments investigating the effects of the D172N mutation, for baseline APs the Ba^{2+}-inhibited I_{K1} was replaced by WT virtual I_{K1}, scaling the magnitude of I_{K1} to restore APD_{90}. In 12 cells from 8 animals, APD_{90} in control Tyrode was 177.3 ± 8.7 ms; once endogenous I_{K1} had been inhibited by Ba^{2+} and replaced in dynamic clamp, APD_{90} was 183.9 ± 9.3 ms ($p > 0.05$ ($p = 0.09$) vs control Tyrode). The resting potential was also restored (−79.8 ± 1.1 mV in control Tyrode and −78.5 ± 0.8 mV in Ba^{2+}+WT virtual I_{K1}; $p > 0.05$ ($p = 0.17$)). For these experiments, we also measured the peak outward I_{K1} inhibited by Ba^{2+} ions during a voltage ramp protocol (460.8 ± 42.6 pA; 4.9 ± 0.4 pA/pF) and compared this with the peak outward virtual I_{K1} supplied in dynamic clamp to restore APD_{90} (599.2 ± 76.4 pA; 6.5 ± 0.8 pA/pF). Although there was a trend for the latter to be greater, this was not statistically significant ($p > 0.05$ for both absolute currents and current densities; paired *t*-test).

The upper panel of **Figure 4Ai** shows exemplar AP traces at 1 Hz with WT, WT-D172N and D172N I_{K1}. The brief depolarizing current pulses supplied to elicit APs were altered as required when the WT I_{K1} formulation was replaced with WT-D712N and D172N formulations. Both heterozygotic and homozygotic D172N I_{K1} formulations led to APD abbreviation, associated with increased I_{K1} amplitude during late repolarization. The mean charge (product of

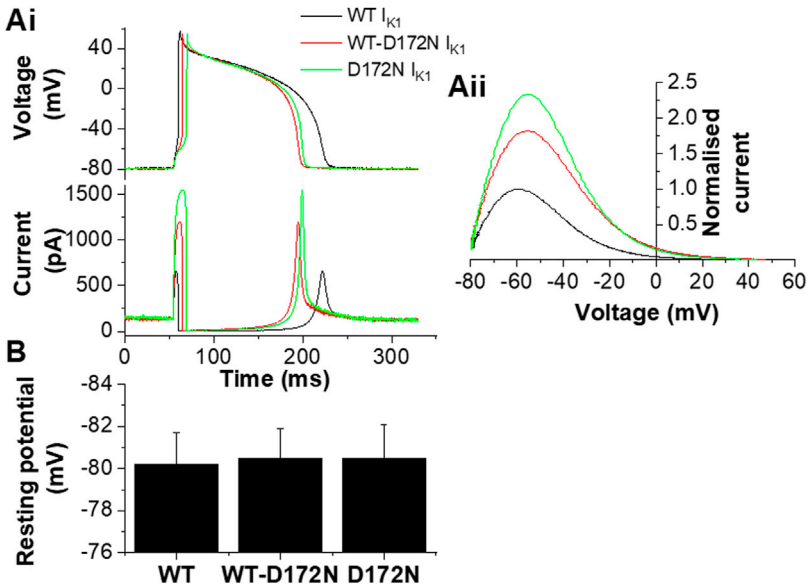

FIGURE 4 | Guinea-pig ventricular APs under dynamic clamp. **Ai**. Guinea-pig ventricular APs elicited from a cell by brief suprathreshold current pulses (applied at 1Hz; 1800 pA for 5, 10 and 14 ms for WT, WT-D172N and D172N conditions respectively). Upper traces show APs and lower traces show corresponding applied I_{K1}. Black traces correspond to WT I_{K1}, red traces correspond to WT-D172N I_{K1}, green traces correspond to D172N I_{K1}. **Aii.** Instantaneous I–V relations for WT, WT-D172N and D172N conditions during the AP repolarization phase (from 10 ms after the AP peak to completion of repolarization; repolarization occurs from right to left on this plot. Currents were normalized to peak outward current with the WT I_{K1} formulation). Peak outward current during AP repolarization occurred at −61.5, −57 and −57 mV respectively. **(B)**. Effects of different I_{K1} formulations on AP resting potential of guinea-pig ventricular myocytes (n = 5 cells from 4 hearts to which each of WT, WT-D172N and D172N I_{K1} were applied).

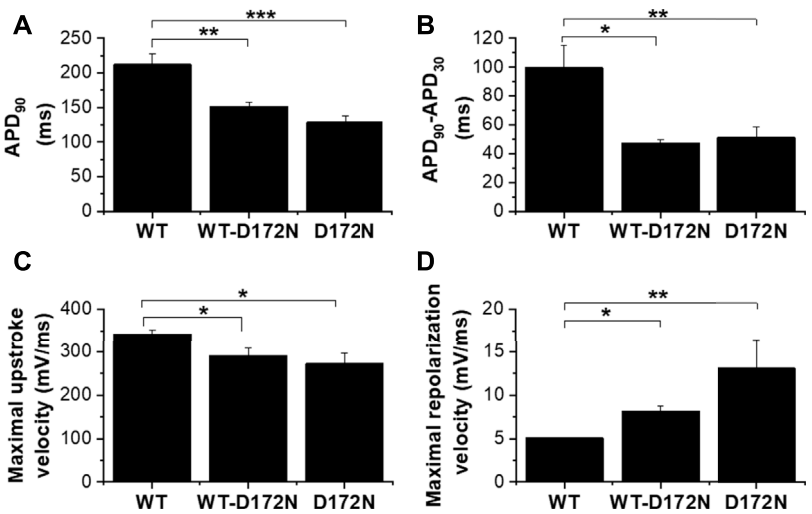

FIGURE 5 | Mean effects of different I_{K1} formulation on guinea-pig ventricular action potential parameters. **(A)**. Mean (±SEM) of APD_{90} values for APs elicited at 1 Hz for WT, WT-D172N and D172N I_{K1} conditions. **(B)**. Mean (±SEM) APD_{90}-APD_{30} values (as an index of AP triangulation) for WT, WT-D172N and D172N I_{K1} conditions. **(C)**. Mean (±SEM) maximal upstroke velocity (V_{max}) values for WT, WT-D172N and D172N I_{K1} conditions. **(D)**. Mean (±SEM) maximal repolarization velocity values for WT, WT-D172N and D172N I_{K1} conditions. "*" denotes statistical significance of $p < 0.05$; "**" denotes statistical significance of $p < 0.01$; "****" denotes statistical significance of $p < 0.001$ (one-way ANOVA test, followed by Tukey's multiple comparisons test; n = 5 cells from 4 hearts to which all I_{K1} formulations were applied).

current amplitude and duration) supplied to elicit APs was 8.7 ± 1.2 pC, 13.3 ± 2.1 pC and 19.0 ± 3.7 pC for WT, WT-D172N and D172N formulations respectively (n = 5; $p < 0.05$ between both mutation conditions and WT; one way ANOVA with Tukey post-test). **Figure 4Aii** shows instantaneous I-V relations for I_{K1} during the AP repolarization phase, which

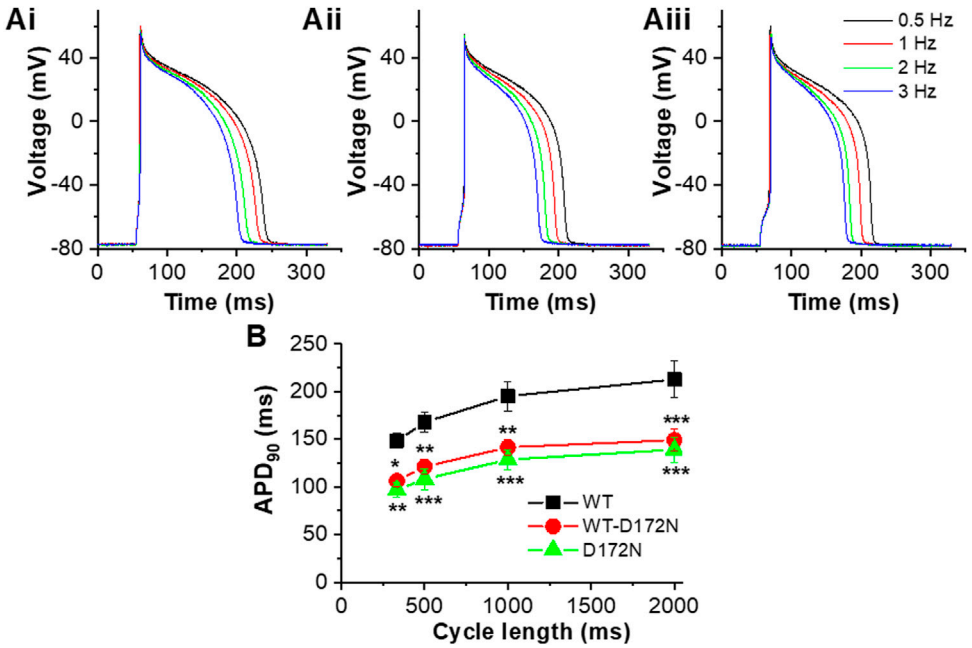

FIGURE 6 | AP rate-dependence for WT, WT-D172N and D172N I_{K1}. **(A)**. Example APs elicited in a single experiment at 4 stimulation frequencies (0.5, 1, 2, 3 Hz) with WT I_{K1} **Ai**, WT-D172N I_{K1} **Aii** and D172N I_{K1} **Aiii**. **(B)**. Plot of APD_{90} against cycle length (1/frequency) for WT I_{K1} (black), WT-D172N I_{K1} (red) and D172N I_{K1} (green) (n = 5 cells from 4 hearts). "*" denotes statistical significance against WT of $p < 0.05$; "**" denotes statistical significance against WT of $p < 0.01$; "***" denotes statistical significance against WT of $p < 0.001$ (two-way ANOVA test, followed by Tukey's multiple comparisons test; n = 5 cells from 4 hearts to which all I_{K1} formulations were applied).

closely resembled those seen with the model cell in **Figure 1Bii**. In addition, a rapid outward I_{K1} transient was seen during the AP that was coincident with the AP upstroke and that differed between WT and mutant conditions (**Figure 4Ai**). This rapid current component is in line with previous experimental observations: a similar transient outward component of native guinea-pig and canine ventricular I_{K1} has been reported previously in experiments employing more classical voltage clamp protocols (Li et al., 1998; Li et al., 2000) and is visible in some of the dynamic clamp I_{K1} records in hiPSC-CM experiments performed by Meijer van Putten et al (2015). As shown in **Figure 4Ai** there appeared to be little change in the resting potential between WT and mutant I_{K1} conditions. This observation was borne out by analysis of mean data from 5 similar experiments in which all 3 I_{K1} formulations were successfully applied to each cell, as no significant difference in resting potential was observed (**Figure 4B**). **Figure 5** shows mean AP parameter data from 5 experiments. **Figure 5A** shows mean APD_{90} values; APD_{90} was significantly abbreviated by both I_{K1} mutant formulations. Replacement of WT I_{K1} with WT-D127N I_{K1} led to a 27.7 ± 2.8% shortening of APD_{90}; although there was a trend towards a greater effect of the D172N I_{K1} formulation (38.0 ± 6.1% shortening compared to WT), this was not statistically significantly different from WT-D172N ($p > 0.05$). Switching from WT to WT-D172N I_{K1} led to a marked reduction in APD triangulation (APD_{90}—APD_{30}, **Figure 5B**), which was not further significantly altered by switching to D172N I_{K1} alone. **Figure 5C** shows maximal AP upstroke velocity (V_{max}) with WT and mutant formulations; there was a modest but significant reduction in V_{max} compared to WT with both heterozygotic and homozygotic D172N formulations. As the current stimuli used to elicit APs were set beyond threshold levels, it was not possible to ascertain whether or not the reduction in V_{max} was accompanied by any significant change in AP threshold voltage. However, peak overshoot potential values were analysed and found to be: 58.2 ± 3.5 mV, 51.7 ± 2.4 mV and 54.0 ± 3.2 mV (n = 5) for WT, WT-D172N and D172N formulations respectively. Although there was a trend towards a reduction in overshoot amplitude with the mutant I_{K1} formulations, this did not reach statistical significance (Friedman test; $p = 0.09$).

Figure 5D shows maximal repolarization velocity under the 3 different conditions. Both heterozygotic and homozygotic D172N formulations led to significant acceleration of terminal repolarization compared to the WT condition; however, whilst there was a trend towards a greater effect of D172N than WT-D172N, this did not attain significance. BVR was 1.6 ± 0.2 ms in control and 1.3 ± 0.1 ms and 1.7 ± 0.3 ms in heterozygous and homozygous conditions respectively ($p > 0.05$, one-way ANOVA test followed by Tukey's multiple comparisons test; n = 5 cells from 4 hearts).

Additional measurements were performed in which APs were elicited at different rates (0.5, 1, 2 and 3 Hz) with the 3 different I_{K1} formulations in turn (exemplar traces are shown in **Figure 6A**). At least 20 APs at each rate were sampled and APD_{90} values from 5

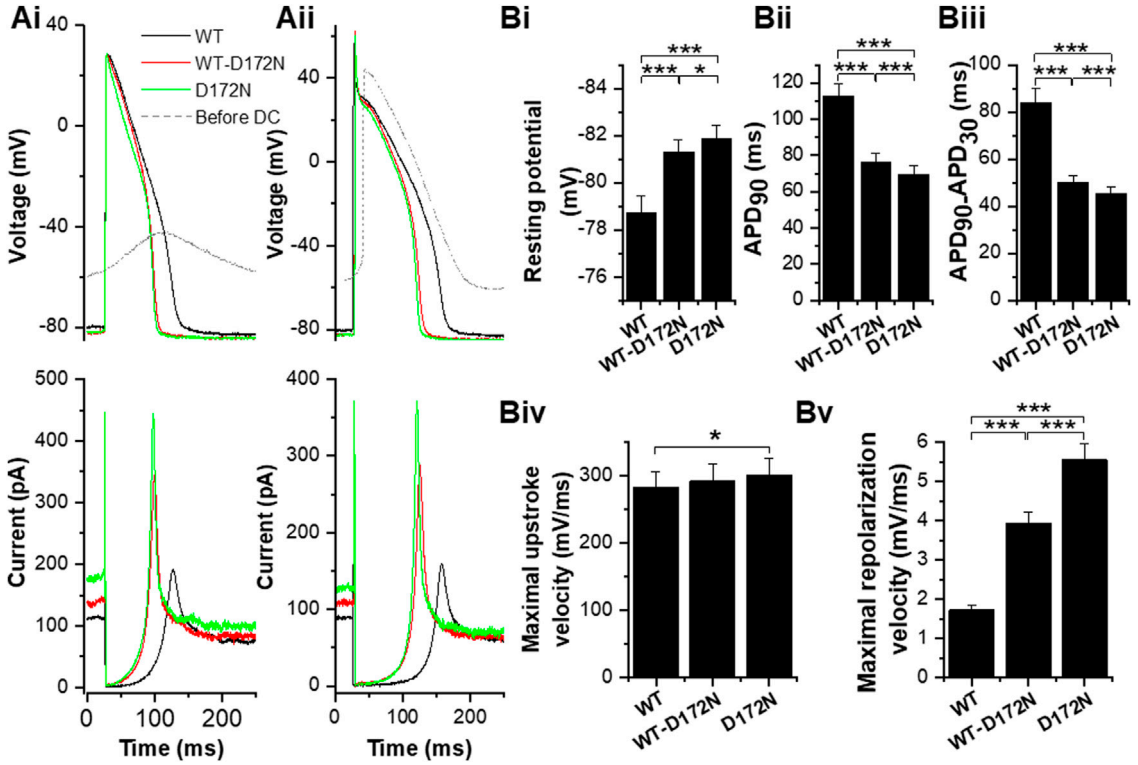

FIGURE 7 | Effects of the D172N-altered I_{K1} on human iPSC-CM APs. **(A)**. Example traces of APs elicited at 1 Hz (by 1.5 ms of 2000 pA current in **Ai**; 1 ms of 2000 pA in **Aii** from iPSC cardiomyocytes to which different I_{K1} formulations were applied (black for WT I_{K1}, red for WT-D172N I_{K1} and green for D172N I_{K1}; superimposed grey traces shows spontaneously oscillating membrane potential (left cell) and spontaneous AP (right cell) prior to activation of the dynamic clamp). Lower traces show corresponding traces of the I_{K1} supplied in each condition. **Bi.** Mean (±SEM) resting potential values for WT, WT-D172N and D172N I_{K1} conditions. **Bii.** Mean (±SEM) maximal APD_{90} values for WT, WT-D172N and D172N I_{K1} conditions. **Biii.** Mean (±SEM) maximal APD_{90}-APD_{30} values (as an index of AP triangulation) for WT, WT-D172N and D172N I_{K1} conditions. **Biv**. Mean (±SEM) maximal upstroke velocity (V_{max}) values for WT, WT-D172N and D172N I_{K1} conditions. **Bv.** Mean (±SEM) maximal repolarization velocity values for WT, WT-D172N and D172N I_{K1} conditions. "*" denotes statistical significance of $p < 0.05$; "***" denotes statistical significance of $p < 0.01$; "****" denotes statistical significance of $p < 0.001$ (one-way ANOVA test, followed by Tukey's multiple comparisons test; n = 14 cells for all).

successive APs at each rate were averaged and pooled to obtain the mean data plots shown in **Figure 6B**. As anticipated as the cycle length was reduced (with each I_{K1} formulation) APs shortened and APD_{90} was accordingly reduced. Switching from WT I_{K1} to either heterozygotic (WT-D172N) or homozygotic (D172N) mutant conditions led to a marked abbreviation of APD_{90} at all rates tested ($p < 0.05$ for WT-D172N and $p < 0.001$ for D172N vs WT respectively; see **Figure 6** legend for significance values from comparison of individual stimulus frequencies between mutant and WT conditions). Thus, introduction of the D172N mutation abbreviated APD_{90} over the entire range of stimulation frequencies examined. There was little difference between the two mutant conditions, however. Due to difficulties in maintaining recordings at high rates, stimulation rates above 3 Hz were not applied and so APD_{90} values at shorter cycle lengths were not obtained.

Effect of Mutant I_{K1} Formulations on the Configuration of APs From hiPSC-Cardiomyocytes

Although the principal focus of this study was on effects of alterations to I_{K1} on APs from adult guinea-pig ventricular myocytes, for comparative purposes a limited series of experiments were conducted at 1 Hz on human iPSC-CMs. COR-4U cardiomyocytes have only low *KCNJ2* expression (Huo et al., 2017). Unpaced COR-4U myocytes have also been reported to exhibit little or no I_{K1} up to 14 days in culture post thaw, with perinuclear staining of Kir2.1 (Gélinas et al., 2017). Moreover, Ba^{2+}-sensitive current recorded from these iPSC-CMs has been reported to have a reversal potential and rectification profile that differ from those expected from a pure I_{K1} (Goversen et al., 2017). The majority of iPSC-CMs from which we recorded (11/14) exhibited spontaneous APs with a mean maximum diastolic potential (MDP) of −54.3 ± 3.6 mV, which would not be expected in the presence of a substantial I_{K1}. In consequence, the different I_{K1} formulations were applied in dynamic clamp experiments without prior application of Ba^{2+} ions and with application of sufficient WT I_{K1} to give a ventricular-like AP configuration and stable resting potential close to −80 mV (−78.7 ± 0.7 mV). In 14 cells APs with the WT I_{K1} formulation were elicited by brief depolarizing current injections (supplying 2.5 ± 0.2 pC; $p <$ 0.001 vs WT I_{K1} guinea-pig ventricular APs, Mann-Whitney

test). The peak outward WT I_{K1} supplied by dynamic clamp during repolarization was 164.4 ± 10.2 pA (3.0 ± 0.1 pA/pF). For each cell, WT-D172N and D172N formulations were then applied at the same fixed ratios as used in guinea-pig myocyte experiments. Changes in the magnitude of the stimulus required to elicit APs were not required when I_{K1} formulations were changed. **Figure 7A** shows exemplar traces of APs elicited at 1 Hz (upper traces) from two iPSC-CMs, with the corresponding applied WT and mutant I_{K1} also shown (lower traces). For completeness, also superimposed are membrane potential recordings from each cell prior to activation of dynamic clamp. The cell in **Figure 7Ai** showed a subthreshold oscillating membrane potential, whilst that in **Figure 7Aii** exhibited spontaneous APs prior to injection of synthetic I_{K1} under dynamic clamp. The I_{K1} profiles under dynamic clamp were qualitatively similar to those seen in guinea-pig myocyte experiments with the clear difference that proportionately greater current was evident during the resting potential [compare, for example, the relative amplitude (ratio) of peak I_{K1} during repolarization with that at the resting potential for the WT I_{K1} records in **Figure 4A** (a ratio of 4.9) and **Figure 7A** (ratios of 1.7 and 1.8 in Ai and Aii)]. This presumably reflects the immature phenotype of the hiPSC-CMs and requirement for I_{K1} to establish a stable negative resting potential. In contrast with the observations from guinea-pig myocytes, the resting potential differed between WT, WT-D172N and D172N conditions, becoming progressively more negative as the amplitude of outward I_{K1} increased due to the mutation (**Figure 7A, Bi**). Although the negative shifts in resting potential were small, they were nevertheless statistically significant. Despite the presence of rapid outward I_{K1} transients during the AP upstroke, upstroke V_{max} did not decrease under mutant conditions (there was no significant difference between WT V_{max} and that with WT-D172N I_{K1}, whilst there was a small but significant increase for D172N I_{K1} alone; **Figure 7Biv**). There was no significant difference in mean overshoot potential between WT, WT-D172N and D172N conditions (53.1 ± 4.2 mV, 51.8 ± 3.7 mV and 51.4 ± 3.5 mV respectively; n = 14, $p > 0.05$ one-way ANOVA). Effects of the D172N mutant I_{K1} formulations on APD_{90} (**Figure 7Bii**) and AP triangulation (**Figure 7Biii**) in iPSC-CMs were similar to those seen in guinea-pig myocytes, with the greatest differences seen on switching from WT to WT-D172N I_{K1} formulations, with small (but significant) additional changes on switching to D172N I_{K1} alone. Analysis of maximum repolarization velocity (**Figure 7Bv**) showed this to be accelerated with the mutant I_{K1} formulations compared to the WT condition.

DISCUSSION

Effects of Ba^{2+} and Establishing the WT Baseline

Although multiple studies have now used dynamic clamp to compensate for the deficit of intrinsic I_{K1} in stem-cell derived cardiomyocytes (e.g., Bett et al., 2013; Meijer van Putten et al., 2015; Goversen et al., 2017; Verkerk et al., 2017; Fabbri et al., 2019; Becker et al., 2020) there is relatively little published work in which I_{K1} has been supplied to isolated adult cardiomyocytes from human-relevant model species using this technique. Dynamic clamp has been used in the exploration of regional differences in I_{K1} shape and magnitude in the canine heart (Cordeiro et al., 2015). A recent study has applied synthetic I_{K1} through dynamic clamp to isolated human atrial myocytes (Verkerk et al., 2021): application of I_{K1} with moderate rectification significantly improved resting potentials, whilst the atrial APs with injected I_{K1} exhibited a sensitivity to blockers of other ion channels that indicated that major ionic currents remained functional (Verkerk et al., 2021). The data from our experiments now show that virtual I_{K1} replacement in adult ventricular myocytes using dynamic clamp facilitates study of the consequences of pathological changes in I_{K1} consequent to an underlying gene mutation, as conducted previously for I_{Kr} and an LQT2 mutation (Berecki et al., 2005).

The concentration of Ba^{2+} ions used here to inhibit I_{K1} (50 μM) is the same as used independently in AP clamp studies to isolate guinea-pig and canine I_{K1} (Banyasz et al., 2011; Horvath et al., 2021). We did not expose myocytes in this study to high (mM) Ba^{2+} concentrations in order to minimize the likelihood of affecting other ionic currents involved in AP genesis. Liu et al (2001) reported K_D values for Ba^{2+} inhibition of I_{K1} of 0.21–1.14 μM between −120 and −80 mV, whilst Schram and others (2003) reported an IC_{50} for I_{K1} block of 4.7 μM. Using that IC_{50} value, 50 μM Ba^{2+} might be predicted to produce ~90% inhibition of the current. Ishihara et al (2002) reported a maximal outward I_{K1} density in guinea-pig ventricular myocytes of 3.1 ± 0.1 pA/pF from perforated patch whole cell recordings; our maximal outward Ba^{2+} sensitive I_{K1} elicited during voltage ramps was 4.9 ± 0.4 pA/pF (albeit under different conditions as we did not use perforated patch recording). Taken together these observations are suggestive that the Ba^{2+} ion concentration used in this study can be expected to have very largely inhibited I_{K1}, though we do not exclude the possibility that a small fraction of the total available current may have remained unblocked. Any residual unblocked component would have been constant during a given dynamic clamp experiment, as 50 μM Ba^{2+} was present throughout these measurements: the control (WT) condition was established by application of sufficient synthetic I_{K1} to restore APD_{90} and then the only subsequent experimental changes made were to substitute the mutant for WT I_{K1} formulations.

Miake *et al* have previously studied the role of I_{K1} in guinea-pig ventricular AP repolarization and in setting resting potential, through overexpression of Kir2.1 and suppression using a dominant negative Kir2.1 construct, the latter reducing outward I_{K1} by 82.1% (Miake et al., 2003). The mean resting potential of transduced ventricular myocytes was hyperpolarized by 4.4 mV with Kir2.1 overexpression, whilst it was depolarized by 6.7 mV with expression of the dominant negative construct to suppress I_{K1} (Miake et al., 2003). Despite these experimental

conditions (transduced, cultured myocytes) differing from those used here, the two studies are in close agreement in the extent of resting membrane potential depolarization with I_{K1} suppression (~7 and ~6 mV respectively). Miake *et al* also reported that dominant negative I_{K1} suppression had a greater effect on APD_{90} than on APD_{50}, slowing repolarization velocity over this time period (Miake et al., 2003). This is in good agreement with the increased AP triangulation seen in the present study with Ba^{2+} application. Beat-to-beat variability in APD_{90} was not evaluated in that study (Miake et al., 2003), so comparisons with our data are not possible in this regard. However, increased short term variability in rat ventricular AP duration has been reported with I_{K1} inhibition (Skarsfeldt et al., 2016), which is consistent with our results. Thus, the effects of I_{K1} inhibition with 50 μM Ba^{2+} in this study are consistent with anticipated effects of substantial I_{K1} reduction.

Application of synthetic I_{K1} in the presence of Ba^{2+} was able to restore APD_{90} and produce APs of a normal morphology, which then provided a baseline for the investigation of effects of the D172N Kir2.1 mutation. Interestingly, the peak amplitude of outward I_{K1} during terminal repolarization supplied under dynamic clamp in the present study is similar to that observed previously for $[K^+]_o$ sensitive I_{K1} from guinea-pig myocytes under AP clamp (Figure 9c of Li et al., 2000). The profile of WT I_{K1} during late AP repolarization in our experiments was as expected and the profile and timing of this current (evident in the instantaneous I-V plot for WT I_{K1}) explain why reduction of I_{K1} predominantly affects late repolarization. The initial rapid outward current component seen during AP depolarization merits some comment, however. As noted in the Results section, a transient outward component of I_{K1} has been reported in guinea-pig and canine myocytes previously (Li et al., 1998; Li et al., 2000). Under AP clamp of ventricular myocytes from both species, the upstroke of the applied AP command elicited a rapid transient I_{K1} [measured as either K_o^+-sensitive or Ba^{2+}-sensitive current; (Li et al., 1998; Li et al., 2000; Li & Dong, 2010)]. Further experiments on recombinant Kir2.1 channels showed that they are also able to generate an early transient outward current component (Zhang et al., 2009). Such transients are consistent with rapid voltage excursions during the AP upstroke through the membrane potential range within which outward I_{K1} occurs. From this and considering the comparatively fast loop time of our dynamic clamp system (see Methods), we infer that at least a part of the initial outward current at the start of the AP was not artifactual.

Effects of the D172N Mutation With Dynamic Clamp–Results in Context

The inward rectification of Kir2.1 depends on three positively charged amino acid residues in the second transmembrane domain (D172), and C terminus (E244 and E299) of the channel (Abrams et al., 1996; Xie et al., 2002; Xie et al., 2003). The D172N mutation reduces the voltage dependent block of the channel responsible for inward rectification, thereby increasing outward Kir2.1 current (Abrams et al., 1996; Priori et al., 2005) (and hence I_{K1}). In the initial report of SQT3 arising from the D172N mutation, simulations using the Priebe-Beuckelmann human ventricular AP model (Priebe and Beuckelmann, 1998) predicted augmented outward I_{K1} leading to APD abbreviation due to effects arising exclusively during late phase repolarization, leading to accelerated terminal repolarization (Priori et al., 2005). Our own subsequent simulation work (Adeniran et al., 2012) using modifications to the ten Tusscher and Panfilov (2006) human ventricular AP model based on experimental data from WT and D172N channels (El Harchi et al., 2009) showed APD shortening arising late in repolarization with steepening of terminal repolarization. Resting potential values were little altered, however, with less than 1 mV of difference in resting potential between the WT and homozygous D172N condition in our simulations (Adeniran et al., 2012). An independent study, using the O'Hara et al (2011) human ventricular AP model showed very similar effects of the D172N mutation in respect of steepening of late AP repolarization and little effect on resting potential (Deo et al., 2013). Steepening of this final AP repolarization phase was shown in multicellular models to account for the asymmetric, tall T waves seen in the SQT3 proband (Priori et al., 2005; Adeniran et al., 2012). Our dynamic clamp data from guinea-pig ventricular myocytes and hiPSC-CMs are therefore consistent with and supportive of the results from prior AP simulations (Priori et al., 2005; Adeniran et al., 2012; Adeniran et al., 2013; Deo et al., 2013), in showing: APD_{90} abbreviation; abbreviation of the APD_{90}-APD_{30} interval; increased maximal repolarization velocity and little change in resting membrane potential. Additionally, our experiments indicated that these changes occurred without any exacerbation of beat-to-beat variability in APD_{90}.

Deo and others predicted the effects of the D172N Kir2.1 mutation on ventricular repolarization to be rather less than those of the SQT3 E299V Kir2.1 mutation reported for the first time in their study (Deo et al., 2013). This is entirely consistent with the much more extensive abolition of current rectification produced by the E299V mutation, which leads to augmented I_{K1} over a greater membrane potential range than does D172N (Deo et al., 2013). In turn, this led to dramatic AP shortening when applied under dynamic clamp to hiPSC-CMs (Meijer van Putten et al., 2015). The D172N mutation produces a less extensive AP abbreviation (as shown in this study and Priori et al., 2005; Adeniran et al., 2012; Adeniran et al., 2013; Deo et al., 2013).

The D172N expressing proband and her father were both heterozygous for this Kir2.1 mutation (Priori et al., 2005) and so any arrhythmic substrate *in vivo* is due to heterozygous and not homozygous expression of the mutation. Accordingly, the findings of this study most relevant to the clinical scenario are those with the heterozygotic WT-D172N I_{K1} formulation. In this regard, it is notable that the biggest change in guinea-pig ventricular AP profile occurred when the WT I_{K1} formulation was switched to the heterozygous WT-D172N formulation, with relatively little additional effect of the homozygous D172N formulation. In our experiments on hiPSC-CMs it was also the case that introduction of the heterozygous WT-D172N formulation had a marked effect on repolarization parameters, with relatively modest increases in most effects on further application of the homozygous D172N formulation.

Collectively, our results on both cell preparations are in fair agreement with ventricular AP simulations from studies in which D172N I_{K1} produced relatively modest further AP abbreviation in comparison to WT-D172N I_{K1} (Priori et al., 2005; Adeniran et al., 2012; Deo et al., 2013). We found that guinea-pig ventricular APD_{90} was abbreviated over a range of stimulation rates by the D172N-containing I_{K1} formulations, shown by the downward shift of the APD_{90}-cycle length relationship in **Figure 6**. This is also in good agreement with prior simulations, which showed that simulated APD-rate or restitution relationships (plotted as APD against diastolic interval/basic cycle length) for D172N conditions were down-ward shifted compared to that for WT I_{K1} (Priori et al., 2005; Adeniran et al., 2012; Deo et al., 2013). In particular the simulations of Deo et al., showed parallel-downward shifted APD-BCL relationships, with a marked effect of heterozygotic incorporation of the D172N mutation and a relatively modest additional effect of the homozygous condition. The shorter APD values over a range of diastolic intervals have been associated in simulations with abbreviated effective refractory periods (ERPs), which contribute to the proarrhythmic substrate in tissue simulations with the D172N mutation (Adeniran et al., 2012). Simulations incorporating very short diastolic intervals/cycle lengths (Adeniran et al., 2012) showed an additional tendency for increase of steepness of maximal slope of APD-restitution. Whilst our experimentally derived APD-rate relationships encompass a range of rates relevant to human repolarization, the requirement to apply successfully multiple stimulation rates with three different I_{K1} formulations prevented us from including stimulation rates >3 Hz.

The modest decrease (<20%) in guinea-pig ventricular AP maximal upstroke velocity seen with the WT-D172N and D172N I_{K1} formulations appears to correlate with the greater opposing early outward transient component of I_{K1} elicited during the AP upstroke. Although this observation has not been highlighted in prior simulations of the effects of D172N on ventricular electrophysiology (Priori et al., 2005; Adeniran et al., 2012; Deo et al., 2013), prominent outward I_{K1} transients during the ventricular AP upstroke have been observed in some simulations of the effect of the D172N Kir2.1 mutation (Adeniran et al., 2013) and a decrease in ventricular conduction velocity (CV) at rates <107 beats min^{-1} was predicted with the mutation by Adeniran et al. (2012) due to reduced tissue excitability. In simulations at high rates tissue CV actually increased, which was thought to be attributable to ERP abbreviation (Adeniran et al., 2012). Notably, we did not see a similar effect in our experiments on hiPSC-CMs: there was a statistically insignificant increase in maximal upstroke velocity under WT-D172N (i.e., clinically relevant) conditions, an effect that became significant for homozygous conditions. hiPSC-CMs also exhibited a modest hyperpolarization in resting potential when WT I_{K1} was exchanged for heterozygotic or homozygotic D172N I_{K1}. It seems likely that these two changes are related and that any effect of hyperpolarizing resting membrane potential on I_{Na} availability may have predominated over any increased early I_{K1} transients, in influencing the AP upstroke velocity. The hyperpolarization of resting potential with D172N-modified I_{K1} in hiPSC-CMs differs both from our results from guinea-pig ventricular myocytes and prior ventricular simulations of effects of the mutation (Priori et al., 2005; Adeniran et al., 2012; Deo et al., 2013). However, simulations of *atrial* effects of the D172N Kir2.1 mutation have shown a modest (up to ~5 mV) hyperpolarization of resting membrane potential together with an (up to ~20 V/s) increase in AP maximal upstroke velocity (Whittaker et al., 2017). Although the hiPSC-CMs that we used exhibited ventricular-like APs when supplied with synthetic I_{K1}, they were derived from a mixed (as opposed to ventricular-like cell enriched) cell preparation. Further, spontaneously active myocytes typically have highly labile membrane potentials over the diastolic potential range (Irisawa et al., 1993; Hancox et al., 2003) and so it is perhaps not surprising that hiPSC-CM resting potential was more sensitive to mutant I_{K1} formulations than that from adult ventricular myocytes. It is also of interest that in dynamic clamp experiments using hiPSC-CMs to study effects of the E299V Kir2.1 mutation Meijer van Putten et al (2015) observed hyperpolarization of MDP when that gain-of-function mutant I_{K1} formulation was introduced.

Potential Limitations and Conclusions

Channels underpinning native I_{K1} involve other Kir2.x isoforms in addition to Kir2.1 (Dhamoon & Jalife, 2005) and modifications to I_{K1} in this study were based solely on changes to Kir2.1 function. However, in the human ventricle Kir2.1 transcript dominates (>90%) over other isoforms (Wang et al., 1998) and the profound effect of Kir2.1 suppression on guinea-pig ventricular I_{K1} (Miake et al., 2003) suggests that Kir2.1 is predominantly responsible for I_{K1} in this species as well. It is therefore reasonable to modify I_{K1} according to alterations to Kir2.1 current properties, as has been implemented in prior SQT3 simulation (Priori et al., 2005; Adeniran et al., 2012; Deo et al., 2013; Whittaker et al., 2017) and dynamic clamp (Meijer van Putten et al., 2015) investigations. The scaling of WT-D172N and D172N formulations relative to WT amplitudes based on I-V data in **Figure 1A** of Adeniran et al (2012) rather than using differences in simulated AP clamp data (**Figure 1B** of that study) was conservative; larger mutation effects on AP parameters, particularly in the homozygotic condition, might have been observed in dynamic clamp experiments in this study had those larger scaling ratios been used. However, D172N mutation carriers were heterozygotic for the mutation (Priori et al., 2005) and so the homozygotic experimental condition is without direct clinical relevance. Native I_{K1} is sensitive to intracellular $[Ca^{2+}]_i$ (Zaza et al., 1998) and there would be no dynamic modulation of I_{K1} by $[Ca^{2+}]_i$ transients for synthetic I_{K1}. However, this limitation would apply also to prior simulation studies and it is notable that: (a) the experimental results observed here are concordant with major AP changes predicted from computational modelling (Priori et al., 2005; Adeniran et al., 2012; Adeniran et al., 2013; Deo et al., 2013), and (b) that tissue models incorporating these AP changes recapitulate ECG changes seen in patients and have shown how substrate(s) for re-entrant arrhythmia may arise (Priori et al., 2005; Adeniran et al., 2012). This highlights that, optimally, dynamic clamp experiments can be used together with cell and tissue

computational modelling, as the combination of these approaches is likely to provide robust insight into cellular effects of channel mutations, with tissue modelling then allowing evaluation of the tissue arrhythmia substrate(s) that is not possible from *in vitro* single cell experiments alone. In the case of D172N Kir2.1, this provides confidence that the simulated AP changes predicating prior predictions of increased temporal vulnerability and reduced minimal substrate size for sustaining reentry in this form of SQT3 are likely to be valid (Adeniran et al., 2012). Another potential limitation, which is inherent in the dynamic clamp approach, is that synthetic currents are not amenable to direct pharmacological modulation, so that it is not possible to investigate directly effects of acute selective pharmacological inhibition on gain-of-function mutations. Nevertheless, our study provides further evidence of the value of dynamic clamp in interrogating functional consequences of Kir2.1-related channelopathies (Meijer van Putten et al., 2015), whilst highlighting the possibility that results from mature adult cardiomyocytes and hiPSC-CMs are likely to be similar, but may not be identical.

DATA AVAILABILITY STATEMENT

The original contributions presented in the study are included in the article/supplementary material, further inquiries can be directed to the corresponding author.

ETHICS STATEMENT

The animal study was reviewed and approved by the University of Bristol AWERB.

AUTHOR CONTRIBUTIONS

JH and HZ conceived and designed the study. RR and GB developed the Cytocybernetics dynamic clamp system and RR, GB, and BF developed and programmed the I_{K1} formulations for the dynamic clamp system. CD conducted and analysed data from electrophysiological experiments. JH and CD drafted the manuscript with input from the other authors.

FUNDING

This study was funded by the British Heart Foundation (PG/15/106/31915 and PG/19/26/34302).

ACKNOWLEDGMENTS

We thank Andrew James and Stephen Harmer for valuable discussion, Stéphanie Choisy, Hongwei Cheng and Rachel Caves for help and advice on cardiomyocyte isolation and Leigh Korbel for help quantifying dynamic clamp speed.

REFERENCES

Abrams, C. J., Davies, N. W., Shelton, P. A., and Stanfield, P. R. (1996). The Role of a Single Aspartate Residue in Ionic Selectivity and Block of a Murine Inward Rectifier K^+ Channel Kir2.1. *J. Physiol.* 493, 643–649. doi:10.1113/jphysiol.1996.sp021411

Adeniran, I., El Harchi, A., Hancox, J. C., and Zhang, H. (2012). Proarrhythmia in KCNJ2-Linked Short QT Syndrome: Insights from Modelling. *Cardiovasc. Res.* 94, 66–76. doi:10.1093/cvr/cvs082

Adeniran, I., Hancox, J. C., and Zhang, H. (2013). In Silico investigation of the Short QT Syndrome, Using Human Ventricle Models Incorporating Electromechanical Coupling. *Front. Physiol.* 4, 166. doi:10.3389/fphys.2013.00166

Ambrosini, E., Sicca, F., Brignone, M. S., D'Adamo, M. C., Napolitano, C., Servettini, I., et al. (2014). Genetically Induced Dysfunctions of Kir2.1 Channels: Implications for Short QT3 Syndrome and Autism-Epilepsy Phenotype. *Hum. Mol. Genet.* 23, 4875–4886. doi:10.1093/hmg/ddu201

Banyasz, T., Horvath, B., Jian, Z., Izu, L. T., and Chen-Izu, Y. (2011). Sequential Dissection of Multiple Ionic Currents in Single Cardiac Myocytes under Action Potential-Clamp. *J. Mol. Cell Cardiol* 50, 578–581. doi:10.1016/j.yjmcc.2010.12.020

Becker, N., Horváth, A., De Boer, T., Fabbri, A., Grad, C., Fertig, N., et al. (2020). Automated Dynamic Clamp for Simulation of Ik1 in Human Induced Pluripotent Stem Cell-Derived Cardiomyocytes in Real Time Using Patchliner Dynamite8. *Curr. Protoc. Pharmacol.* 88, e70. doi:10.1002/cpph.70

Berecki, G., Zegers, J. G., Verkerk, A. O., Bhuiyan, Z. A., de Jonge, B., Veldkamp, M. W., et al. (2005). hERG Channel (Dys)function Revealed by Dynamic Action Potential Clamp Technique. *Biophys. J.* 88, 566–578. doi:10.1529/biophysj.104.047290

Bett, G. C., Kaplan, A. D., Lis, A., Cimato, T. R., Tzanakakis, E. S., Zhou, Q., et al. (2013). Electronic "expression" of the Inward Rectifier in Cardiocytes Derived from Human-Induced Pluripotent Stem Cells. *Heart Rhythm* 10, 1903–1910. doi:10.1016/j.hrthm.2013.09.061

Cordeiro, J. M., Zeina, T., Goodrow, R., Kaplan, A. D., Thomas, L. M., Nesterenko, V. V., et al. (2015). Regional Variation of the Inwardly Rectifying Potassium Current in the Canine Heart and the Contributions to Differences in Action Potential Repolarization. *J. Mol. Cell Cardiol* 84, 52–60. doi:10.1016/j.yjmcc.2015.04.010

Deo, M., Ruan, Y., Pandit, S. V., Shah, K., Berenfeld, O., Blaufox, A., et al. (2013). KCNJ2 Mutation in Short QT Syndrome 3 Results in Atrial Fibrillation and Ventricular Proarrhythmia. *Proc. Natl. Acad. Sci. U S A.* 110, 4291–4296. doi:10.1073/pnas.1218154110

Dhamoon, A. S., and Jalife, J. (2005). The Inward Rectifier Current (Ik1) Controls Cardiac Excitability and Is Involved in Arrhythmogenesis. *Heart Rhythm* 2, 316–324. doi:10.1016/j.hrthm.2004.11.012

Doss, M. X., Di Diego, J. M., Goodrow, R. J., Wu, Y., Cordeiro, J. M., Nesterenko, V. V., et al. (2012). Maximum Diastolic Potential of Human Induced Pluripotent Stem Cell-Derived Cardiomyocytes Depends Critically on I_{Kr}. *PLoS One* 7, e40288. doi:10.1371/journal.pone.0040288

El Harchi, A., McPate, M. J., Zhang, Y. H., Zhang, H., and Hancox, J. C. (2009). Action Potential Clamp and Chloroquine Sensitivity of Mutant Kir2.1 Channels Responsible for Variant 3 Short QT Syndrome. *J. Mol. Cell Cardiol* 47, 743–747. doi:10.1016/j.yjmcc.2009.02.027

El-Battrawy, I., Lan, H., Cyganek, L., Zhao, Z., Li, X., Buljubasic, F., et al. (2018). Modeling Short QT Syndrome Using Human-Induced Pluripotent Stem Cell-Derived Cardiomyocytes. *J. Am. Heart Assoc.* 7, e007394. doi:10.1161/JAHA.117.007394

Fabbri, A., Goversen, B., Vos, M. A., van Veen, T. A. B., and de Boer, T. P. (2019). Required GK1 to Suppress Automaticity of iPSC-CMs Depends Strongly on Ik1 Model Structure. *Biophys. J.* 117, 2303–2315. doi:10.1016/j.bpj.2019.08.040

Gaborit, N., Le Bouter, S., Szuts, V., Varro, A., Escande, D., Nattel, S., et al. (2007). Regional and Tissue Specific Transcript Signatures of Ion Channel Genes in the Non-diseased Human Heart. *J. Physiol.* 582, 675–693. doi:10.1113/jphysiol.2006.126714

Gélinas, R., El Khoury, N., Chaix, M. A., Beauchamp, C., Alikashani, A., Ethier, N., et al. (2017). Characterization of a Human Induced Pluripotent Stem Cell-

Derived Cardiomyocyte Model for the Study of Variant Pathogenicity: Validation of a KCNJ2 Mutation. *Circ. Cardiovasc. Genet.* 10, e001755. doi:10.1161/CIRCGENETICS.117.001755

Goversen, B., Becker, N., Stoelzle-Feix, S., Obergrussberger, A., Vos, M. A., van Veen, T. A. B., et al. (2017). A Hybrid Model for Safety Pharmacology on an Automated Patch Clamp Platform: Using Dynamic Clamp to Join iPSC-Derived Cardiomyocytes and Simulations of Ik1 Ion Channels in Real-Time. *Front. Physiol.* 8, 1094. doi:10.3389/fphys.2017.01094

Guo, F., Sun, Y., Wang, X., Wang, H., Wang, J., Gong, T., et al. (2018). Patient-Specific and Gene-Corrected Induced Pluripotent Stem Cell-Derived Cardiomyocytes Elucidate Single-Cell Phenotype of Short QT Syndrome. *Circ. Res.* 124, 66–78. doi:10.1161/CIRCRESAHA.118.313518

Hancock, J. M., Weatherall, K. L., Choisy, S. C., James, A. F., Hancox, J. C., and Marrion, N. V. (2015). Selective Activation of Heteromeric SK Channels Contributes to Action Potential Repolarization in Mouse Atrial Myocytes. *Heart Rhythm* 12, 1003–1015. doi:10.1016/j.hrthm.2015.01.027

Hancox, J. C., Whittaker, D. G., Du, C., Stuart, A. G., and Zhang, H. (2018). Emerging Therapeutic Targets in the Short QT Syndrome. *Expert Opin. Ther. Targets* 22, 439–451. doi:10.1080/14728222.2018.1470621

Hancox, J. C., Whittaker, D. G., Zhang, H., and Stuart, A. G. (2019). Learning from Studying Very Rare Cardiac Conditions: the Example of Short QT Syndrome. *J. Congenit. Heart Dis.* 3, 3. doi:10.1186/s40949-019-0024-7

Hancox, J. C., Yuill, K. H., Mitcheson, J. S., and Convery, M. K. (2003). Progress and Gaps in Understanding the Electrophysiological Properties of Morphologically normal Cells from the Cardiac Atrioventricular Node. *Int. J. Bifurcation Chaos* 13, 3675–3691. doi:10.1142/s021812740300879x

Hattori, T., Makiyama, T., Akao, M., Ehara, E., Ohno, S., Iguchi, M., et al. (2012). A Novel Gain-Of-Function KCNJ2 Mutation Associated with Short-QT Syndrome Impairs Inward Rectification of Kir2.1 Currents. *Cardiovasc. Res.* 93, 666–673. doi:10.1093/cvr/cvr329

Hibino, H., Inanobe, A., Furutani, K., Murakami, S., Findlay, I., and Kurachi, Y. (2010). Inwardly Rectifying Potassium Channels: Their Structure, Function, and Physiological Roles. *Physiol. Rev.* 90, 291–366. doi:10.1152/physrev.00021.2009

Hoekstra, M., Mummery, C. L., Wilde, A. A., Bezzina, C. R., and Verkerk, A. O. (2012). Induced Pluripotent Stem Cell Derived Cardiomyocytes as Models for Cardiac Arrhythmias. *Front. Physiol.* 3, 346. doi:10.3389/fphys.2012.00346

Hondeghem, L. M., Carlsson, L., and Duker, G. (2001). Instability and Triangulation of the Action Potential Predict Serious Proarrhythmia, but Action Potential Duration Prolongation Is Antiarrhythmic. *Circulation* 103, 2004–2013. doi:10.1161/01.cir.103.15.2004

Horváth, B., Kiss, D., Dienes, C., Hézső, T., Kovács, Z., Szentandrássy, N., et al. (2021). Ion Current Profiles in Canine Ventricular Myocytes Obtained by the "onion Peeling" Technique. *J. Mol. Cell Cardiol* 158, 153–162. doi:10.1016/j.yjmcc.2021.05.011

Huo, J., Kamalakar, A., Yang, X., Word, B., Stockbridge, N., Lyn-Cook, B., et al. (2017). Evaluation of Batch Variations in Induced Pluripotent Stem Cell-Derived Human Cardiomyocytes from 2 Major Suppliers. *Toxicol. Sci.* 156, 25–38. doi:10.1093/toxsci/kfw235

Irisawa, H., Brown, H. F., and Giles, W. (1993). Cardiac Pacemaking in the Sinoatrial Node. *Physiol. Rev.* 73, 197–227. doi:10.1152/physrev.1993.73.1.197

Ishihara, K., and Ehara, T. (1998). A Repolarization-Induced Transient Increase in the Outward Current of the Inward Rectifier K+ Channel in guinea-pig Cardiac Myocytes. *J. Physiol.* 510, 755–771. doi:10.1111/j.1469-7793.1998.755bj.x

Ishihara, K., Yan, D. H., Yamamoto, S., and Ehara, T. (2002). Inward Rectifier K(+) Current under Physiological Cytoplasmic Conditions in guinea-pig Cardiac Ventricular Cells. *J. Physiol.* 540, 831–841. doi:10.1113/jphysiol.2001.013470

James, A. F., Arberry, L. A., and Hancox, J. C. (2004). Gender-related Differences in Ventricular Myocyte Repolarization in the guinea Pig. *Basic Res. Cardiol.* 99, 183–192. doi:10.1007/s00395-003-0451-6

Jones, D. K., Liu, F., Vaidyanathan, R., Eckhardt, L. L., Trudeau, M. C., and Robertson, G. A. (2014). hERG 1b Is Critical for Human Cardiac Repolarization. *Proc. Natl. Acad. Sci. U S A.* 111, 18073–18077. doi:10.1073/pnas.1414945111

Li, G-R., and Dong, M-Q. (2010). Revisit of the Cardiac Inward Rectifier Potassium Current I_{k1}. *Open Circ. Vasc. J.* 3, 95–102. doi:10.2174/1877382601003010095

Li, G. R., Sun, H., and Nattel, S. (1998). Characterization of a Transient Outward K+ Current with Inward Rectification in Canine Ventricular Myocytes. *Am. J. Physiol.* 274, C577–C585. doi:10.1152/ajpcell.1998.274.3.C577

Li, G. R., Yang, B., Sun, H., and Baumgarten, C. M. (2000). Existence of a Transient Outward K(+) Current in guinea Pig Cardiac Myocytes. *Am. J. Physiol. Heart Circ. Physiol.* 279, H130–H138. doi:10.1152/ajpheart.2000.279.1.H130

Lieu, D. K., Fu, J. D., Chiamvimonvat, N., Tung, K. C., McNerney, G. P., Huser, T., et al. (2013). Mechanism-based Facilitated Maturation of Human Pluripotent Stem Cell-Derived Cardiomyocytes. *Circ. Arrhythm Electrophysiol.* 6, 191–201. doi:10.1161/CIRCEP.111.973420

Liu, G. X., Derst, C., Schlichthörl, G., Heinen, S., Seebohm, G., Brüggemann, A., et al. (2001). Comparison of Cloned Kir2 Channels with Native Inward Rectifier K+ Channels from guinea-pig Cardiomyocytes. *J. Physiol.* 532, 115–126. doi:10.1111/j.1469-7793.2001.0115g.x

Maury, P., Extramiana, F., Sbragia, P., Giustetto, C., Schimpf, R., Duparc, A., et al. (2008). Short QT Syndrome. Update on a Recent Entity. *Arch. Cardiovasc. Dis.* 101, 779–786. doi:10.1016/j.acvd.2008.08.009

McPate, M. J., Zhang, H., Ideniran, I., Cordeiro, J. M., Witchel, H. J., and Hancox, J. C. (2009). Comparative Effects of the Short QT N588K Mutation at 37°C on hERG K^+ Channel Current during Ventricular, Purkinje Fibre and Atrial Action Potentials: an Action Potential Clamp Study. *J. Physiol. Pharmacol.* 60, 23–41.

Meijer van Putten, R. M. E., Mengarelli, I., Guan, K., Zegers, J. G., van Ginneken, A. C., Verkerk, A. O., et al. (2015). Ion Channelopathies in Human Induced Pluripotent Stem Cell Derived Cardiomyocytes: a Dynamic Clamp Study with Virtual Ik1. *Front. Physiol.* 6, 7. doi:10.3389/fphys.2015.00007

Miake, J., Marbán, E., and Nuss, H. B. (2003). Functional Role of Inward Rectifier Current in Heart Probed by Kir2.1 Overexpression and Dominant-Negative Suppression. *J. Clin. Invest.* 111, 1529–1536. doi:10.1172/JCI17959

Mitcheson, J. S., and Hancox, J. C. (1999). An Investigation of the Role Played by the E-4031-Sensitive (Rapid Delayed Rectifier) Potassium Current in Isolated Rabbit Atrioventricular Nodal and Ventricular Myocytes. *Pflugers Arch.* 438, 843–850. doi:10.1007/s004249900118

Mitcheson, J. S., and Sanguinetti, M. C. (1999). Biophysical Properties and Molecular Basis of Cardiac Rapid and Slow Delayed Rectifier Potassium Channels. *Cell Physiol Biochem* 9, 201–216. doi:10.1159/000016317

Noujaim, S. F., Pandit, S. V., Berenfeld, O., Vikstrom, K., Cerrone, M., Mironov, S., et al. (2007). Up-regulation of the Inward Rectifier K^+ Current (I_{k1}) in the Mouse Heart Accelerates and Stabilizes Rotors. *J. Physiol.* 578, 315–326. doi:10.1113/jphysiol.2006.121475

O'Hara, T., Virág, L., Varró, A., and Rudy, Y. (2011). Simulation of the Undiseased Human Cardiac Ventricular Action Potential: Model Formulation and Experimental Validation. *PLOS Comput. Biol.* 7 (5), e1002061. doi:10.1371/journal.pcbi.1002061

Pérez-Riera, A. R., Barbosa-Barros, R., Samesina, N., Pastore, C. A., Scanavacca, M., Daminello-Raimundo, R., et al. (2021). Andersen-Tawil Syndrome: A Comprehensive Review. *Cardiol. Rev.* 29, 165–177. doi:10.1097/CRD.0000000000000326

Priebe, L., and Beuckelmann, D. J. (1998). Simulation Study of Cellular Electric Properties in Heart Failure. *Circ. Res.* 82, 1206–1223. doi:10.1161/01.res.82.11.1206

Priori, S. G., Pandit, S. V., Rivolta, I., Berenfeld, O., Ronchetti, E., Dhamoon, A., et al. (2005). A Novel Form of Short QT Syndrome (SQT3) Is Caused by a Mutation in the KCNJ2 Gene. *Circ. Res.* 96, 800–807. doi:10.1161/01.RES.0000162101.76263.8c

Ridley, J. M., Milnes, J. T., Zhang, Y. H., Witchel, H. J., and Hancox, J. C. (2003). Inhibition of HERG K+ Current and Prolongation of the guinea-pig Ventricular Action Potential by 4-aminopyridine. *J. Physiol.* 549, 667–672. doi:10.1113/jphysiol.2003.043976

Sanson, C., Schombert, B., Filoche-Rommé, B., Partiseti, M., and Bohme, G. A. (2019). Electrophysiological and Pharmacological Characterization of Human Inwardly Rectifying Kir2.1 Channels on an Automated Patch-Clamp Platform. *Assay Drug Dev. Technol.* 17, 89–99. doi:10.1089/adt.2018.882

Schram, G., Pourrier, M., Wang, Z., White, M., and Nattel, S. (2003). Barium Block of Kir2 and Human Cardiac Inward Rectifier Currents: Evidence for Subunit-Heteromeric Contribution to Native Currents. *Cardiovasc. Res.* 59, 328–338. doi:10.1016/s0008-6363(03)00366-3

Shimoni, Y., Clark, R. B., and Giles, W. R. (1992). Role of an Inwardly Rectifying Potassium Current in Rabbit Ventricular Action Potential. *J. Physiol.* 448, 709–727. doi:10.1113/jphysiol.1992.sp019066

Skarsfeldt, M. A., Carstensen, H., Skibsbye, L., Tang, C., Buhl, R., Bentzen, B. H., et al. (2016). Pharmacological Inhibition of Ik1 by PA-6 in Isolated Rat Hearts Affects Ventricular Repolarization and Refractoriness. *Physiol. Rep.* 4, e12734. doi:10.14814/phy2.12734

Takanari, H., Nalos, L., Stary-Weinzinger, A., de Git, K. C., Varkevisser, R., Linder, T., et al. (2013). Efficient and Specific Cardiac Ik_1 Inhibition by a New Pentamidine Analogue. *Cardiovasc. Res.* 99, 203–214. doi:10.1093/cvr/cvt103

Tamargo, J., Caballero, R., Gómez, R., Valenzuela, C., and Delpón, E. (2004). Pharmacology of Cardiac Potassium Channels. *Cardiovasc. Res.* 62, 9–33. doi:10.1016/j.cardiores.2003.12.026

ten Tusscher, K. H., Noble, D., Noble, P. J., and Panfilov, A. V. (2004). A Model for Human Ventricular Tissue. *Am. J. Physiol. Heart Circ. Physiol.* 286, H1573–H1589. doi:10.1152/ajpheart.00794.2003

ten Tusscher, K. H., and Panfilov, A. V. (2006). Alternans and Spiral Breakup in a Human Ventricular Tissue Model. *Am. J. Physiol. Heart Circ. Physiol.* 291, H1088–H1100. doi:10.1152/ajpheart.00109.2006

Tristani-Firouzi, M., and Etheridge, S. P. (2010). Kir 2.1 Channelopathies: the Andersen-Tawil Syndrome. *Pflugers Arch.* 460, 289–294. doi:10.1007/s00424-010-0820-6

Valentin, J. P., Hoffmann, P., De Clerck, F., Hammond, T. G., and Hondeghem, L. (2004). Review of the Predictive Value of the Langendorff Heart Model (Screenit System) in Assessing the Proarrhythmic Potential of Drugs. *J. Pharmacol. Toxicol. Methods* 49, 171–181. doi:10.1016/j.vascn.2004.03.008

Varró, A., Tomek, J., Nagy, N., Virag, L., Passini, E., Rodriguez, B., et al. (2020). Cardiac Transmembrane Ion Channels and Action Potentials: Cellular Physiology and Arrhythmogenic Behavior. *Physiol. Rev.* 101, 1083–1176. doi:10.1152/physrev.00024.2019

Verkerk, A. O., Marchal, G. A., Zegers, J. G., Kawasaki, M., Driessen, A. H. G., Remme, C. A., et al. (2021). Patch-Clamp Recordings of Action Potentials from Human Atrial Myocytes: Optimization through Dynamic Clamp. *Front. Pharmacol.* 12, 649414. doi:10.3389/fphar.2021.649414

Verkerk, A. O., Veerman, C. C., Zegers, J. G., Mengarelli, I., Bezzina, C. R., and Wilders, R. (2017). Patch-Clamp Recording from Human Induced Pluripotent Stem Cell-Derived Cardiomyocytes: Improving Action Potential Characteristics through Dynamic Clamp. *Int. J. Mol. Sci.* 18, 1873. doi:10.3390/ijms18091873

Wang, Z., Yue, L., White, M., Pelletier, G., and Nattel, S. (1998). Differential Distribution of Inward Rectifier Potassium Channel Transcripts in Human Atrium versus Ventricle. *Circulation* 98, 2422–2428. doi:10.1161/01.cir.98.22.2422

Whittaker, D. G., Ni, H., El Harchi, A., Hancox, J. C., and Zhang, H. (2017). Atrial Arrhythmogenicity of KCNJ2 Mutations in Short QT Syndrome: Insights from Virtual Human Atria. *Plos Comput. Biol.* 13, e1005593. doi:10.1371/journal.pcbi.1005593

Xia, M., Jin, Q., Bendahhou, S., He, Y., Larroque, M. M., Chen, Y., et al. (2005). A Kir2.1 Gain-Of-Function Mutation Underlies Familial Atrial Fibrillation. *Biochem. Biophys. Res. Commun.* 332, 1012–1019. doi:10.1016/j.bbrc.2005.05.054

Xie, L. H., John, S. A., and Weiss, J. N. (2003). Inward Rectification by Polyamines in Mouse Kir2.1 Channels: Synergy between Blocking Components. *J. Physiol.* 550, 67–82. doi:10.1113/jphysiol.2003.043117

Xie, L. H., John, S. A., and Weiss, J. N. (2002). Spermine Block of the strong Inward Rectifier Potassium Channel Kir2.1: Dual Roles of Surface Charge Screening and Pore Block. *J. Gen. Physiol.* 120, 53–66. doi:10.1085/jgp.20028576

Zaza, A., Rocchetti, M., Brioschi, A., Cantadori, A., and Ferroni, A. (1998). Dynamic Ca2+-Induced Inward Rectification of K+ Current during the Ventricular Action Potential. *Circ. Res.* 82, 947–956. doi:10.1161/01.res.82.9.947

Zhang, D. Y., Lau, C. P., and Li, G. R. (2009). Human Kir2.1 Channel Carries a Transient Outward Potassium Current with Inward Rectification. *Pflugers Arch.* 457, 1275–1285. doi:10.1007/s00424-008-0608-0

Zhang, Y. H., James, A. F., and Hancox, J. C. (2001). Regulation by Endothelin-1 of Na^+-Ca^{2+} Exchange Current (I_{NaCa}) from guinea-pig Isolated Ventricular Myocytes. *Cell Calcium* 30, 351–360. doi:10.1054/ceca.2001.0244

Conflict of Interest: RR and GB are founders and owners of Cytocybernetics Inc. BF was employed by the company Cytocybernetics Inc.

The remaining authors declare that the research was conducted in the absence of any commercial or financial relationships that could be construed as a potential conflict of interest.

Publisher's Note: All claims expressed in this article are solely those of the authors and do not necessarily represent those of their affiliated organizations, or those of the publisher, the editors and the reviewers. Any product that may be evaluated in this article, or claim that may be made by its manufacturer, is not guaranteed or endorsed by the publisher.